Separation and Purification Technology 313 (2023) 123457

Contents lists available at ScienceDirect

Separation and Purification Technology

journal homepage: www.elsevier.com/locate/seppur

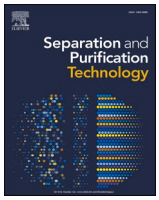

Fixed-bed columns mathematical modeling for selective nickel and copper recovery from industrial spent acids by chelating resins

A. Bringas, E. Bringas, R. Ibañez, Ma.-F. San-Román *

Departamento de Ingenierías Química y Biomolecular, ETSIIyT, Universidad de Cantabria, Avda. de los Castros, 46, Santander 39005, Cantabria, Spain

ARTICLE INFO

Keywords:
Industrial spent acids
Adsorption and desorption
Nickel and copper recovery
Chelating resins
Modeling of fixed-bed columns

ABSTRACT

Spent acid streams generated in industry containing high concentrations of heavy metals are potential secondary sources of raw materials. Chelating resins are excellent candidates to recover valuable metals from complex mixtures at very low pH conditions. In particular, previous works reported high recoveries of nickel and copper from real industrial acids (3400 mg Cu^{2+} L^{-1}, 8700 mg Ni^{2+} L^{-1} and 24000 mg Fe L^{-1}) using commercial bis-picolyamine (BPA)-based resins. In this work, adsorption and desorption using two in-series fixed-bed columns with BPA resins have been proposed to carry out the selective and independent separation and recovery of nickel and copper. Under the selected operating conditions, it was possible to recover 90% of the copper and 80% of the nickel present in the problem solution. A mathematical model based on mass transfer was developed in order to describe the adsorption and desorption stages. Adsorption chemical reactions were modeled as equilibrium reactions, fitting to Langmuir's and Freundlich's isotherms for copper and nickel respectively. The chemical reactions for both metals in desorption fitted into first order reactions. Finally, the kinetic constants k_{de}=0.81 $kg_{dryresin}$ L^{-1} h^{-1} for copper and k_{de}=1.10 $kg_{dryresin}$ L^{-1} h^{-1} for nickel were estimated using the software Aspen Custom modeler. The predicted values agreed with the experimental data.

1. Introduction

The concept of "Responsible Consumption and Production" (Goal 12) appears in the list of Sustainable Development Goals (SDGs) established by the United Nation member states in 2015 as a universal call to end poverty, protect the planet and ensure that all people enjoy peace and prosperity by 2030 [1]. This goal, which is based on achieving sustainable management and efficient use of resources, promotes the need to replace the current model of linear economy, consisting of "take, make and dispose", since it has reached its physical limits, due to the depletion of primary sources of raw materials and the large volume of waste generated [2,3]. Therefore, the implementation of circular economy, defined by the Ellen MacArthur Foundation [4] as a restorative and regenerative industrial economy model, that aims to ensure that products, components and resources in general maintain their usefulness and value at all times, is a promising alternative.

Industrial wastes, especially those with high metal content, are susceptible to be managed from the circular economy point of view, thus becoming secondary sources of raw materials. These hazardous wastes may cause severe environmental problems and health disorders and must be treated before their discharge into the aquatic environment [5]. It is estimated that around $3{\cdot}10^5$ m^3 per year of exhausted industrial baths are produced in Europe, with an average metal content about 40–45 kg m^{-3} [6-8]. Thus, their comprehensive recycling and reintroduction into new lifecycles help to ensure Europés access to key metals, which implies a building block for a competitive economy [9,10]. In this regard, spent acid solutions containing high concentrations of acids and metals are good candidates to be managed following the principles of circular economy, thus solving simultaneously two problems, the reduction of heavy metals concentrations below permissible limits and their recovery for future reuse. The selective recovery of target metals from complex wastes is complicated since metallic compounds are usually dissolved together with large amounts of iron at different concentration levels [8,9,11]. The management of this type of spent acids has been analyzed using different technologies such as membrane processes [12,13], electrolytic methods [14], solvent extraction [15], chemical precipitation [16], coagulation-flocculation [17], ion exchange [18] or adsorption and bioadsorption [14,19-21]. In particular,

* Corresponding author at: Departamento de Ingenierías Química y Biomolecular, ETSIIyT, Universidad de Cantabria, Avda. de los Castros, 46, Santander 39005, Cantabria, Spain.
E-mail address: sanromm@unican.es (Ma.-F. San-Román).

https://doi.org/10.1016/j.seppur.2023.123457
Received 31 December 2022; Received in revised form 14 February 2023; Accepted 20 February 2023
Available online 23 February 2023

ion exchange and adsorption have been widely referred to as suitable technologies for the removal and recovery of heavy metals from industrial effluents due to several advantages such as high selectivity, fast reaction kinetics, low cost, easy operation, high efficiency and minimal generation of sludge [9,22,23]. Despite commercial resins such as Dowex 1X8, Amberlite IR 400 or Purolite S-957 have been confirmed as excellent separation agents to remove heavy metals, their efficiency at extremely low pH values is limited [24,25]. This limitation can be overcome by using polymeric chelating resins containing functional groups capable to form stable complexes with metallic ions by a dative covalent bonding [26]. These kinds of resins are much more selective than conventional ones, and are used very efficiently in preconcentration of metals or recycling processes on an industrial scale, as they have been specially developed for the separation of transition metals particularly from complex matrices, where large concentrations of metal ions are present even at pH values lower than 1.0 [27]. So, Pérez et al. [28] investigated the recovery of copper from a synthetic solution that simulates the limonite ore leach, which, besides, contains nickel, using a continuous process with the chelating resin Dowex XUS 43605, showing that the solution obtained from elution had a copper concentration values 10 times higher than in the loading. Purolite S930 and S950 were tested by Deepatana et al. [29] for the recovery of nickel and cobalt from a synthetic solution that simulates pregnant bioleaching solutions, obtaining favorable adsorption percentages of nickel and cobalt. A new chelating resin synthesized in the reaction of poly (MVE-alt-MA) polymer with a Schiff base obtained in condensation of 2-acetylpyridine and 4-aminobenzoic hydrazide showed effective removal of heavy metal ions, including Cu^{2+}, Cd^{2+}, Cr^{3+}, Ni^{2+} and Co^{2+} from real wastewater samples [30]. Marin and coworkers [31] removed some metal ions including Ni^{2+} and Cu^{2+} from complex mixtures with the resins Amberlite IRA 402 and Amberlite XAD7HP chelated with DR23 using synthetic solutions. Duan and coworkers [32] studied the adsorption mechanism of Ni^{2+} and Cu^{2+} using a PAPDA resin containing –CONHOH and –COOH from simulated electroplating wastewater, Finally, Wolowicz and coworkers [33] evaluated the efficiency of a chelating resin, similar to use in this work, functionalized with bis-picolylamine groups, for the selective adsorption of metal ions including Ni^{2+} and Cu^{2+} from a synthetic mixture. It is worth mentioning that most of the works reported in the literature confirm that the operation pH value is very significant for the performance of chelating resins.

Ulloa and co-workers [8,9] employed the commercial resin Puromet™ MTS9600 functionalized with bis-picolylamine groups in the selective separation of nickel and copper over iron from waste acidic effluents in sulfate media. At pH=2.0, removal percentages of nickel, copper and iron of ≈80%, ≈99% and ≈10% respectively, were reported. Using 2.0 M H_2SO_4 42.8% of nickel was desorbed, while the elution of copper was negligible. However, 2.0 M NH_4OH reported the best results for copper elution with desorption percentages of 97.6% and a negligible elution of nickel.

The theoretical description of the dynamic behavior of the adsorption and desorption process in fixed-bed columns is an essential step to carry out the design and optimization of the process. The rigorous prediction of adsorption and regeneration breakthrough curves requires the development of mathematical models based on mass transfer, chemical reaction and thermodynamic equilibrium, capable of simulating the dynamic behavior of the column, without the need to carry out extensive experimentation, which tends to be expensive and time-consuming [34,35]. The microscopic mass transfer models are usually derived from the Fick's Law and consider the exchange equilibrium and external diffusion, internal diffusion, diffusion in the pore, the diffusion model combined surface and pore, and intraparticle diffusion, among others [36,37]. Finally, in chemical reaction models, the resistance to mass transfer is expressed in terms of a chemical reaction or reaction rate [38].

In this work, adsorption with chelating resins has been selected as the most suitable technique to carry out the selective separation and recovery of copper and nickel present in a real spent acid provided by a waste management company. The main novelty of this work lies in the application and accurate mathematical modeling of the adsorption and regeneration stages in fixed-bed processes applied to the treatment of real spent acids generated in industrial processes. Therefore, the research represents a step forward to previous results obtained with synthetic solutions as previously has been reported. Starting with this study case and considering the previous results, this work has as a general objective the experimental and theoretical validation of the separation-recovery of copper and nickel using fixed-bed columns charged with the chelating resin Puromet™ MTS9600 operating in a continuous mode. In order to provide valuable tools for the design and scaling up of the process, the mathematical modeling of the loading and regeneration steps in the fixed-bed column was developed by describing the mass transfer phenomena and the interfacial interaction between bis-picolylamine groups and the target metals.

2. Experimental section

2.1. Materials section

In the present work, adsorption technology with chelating resins has been applied to a real spent acid supplied by a local company with the composition shown in Table 1 where iron, nickel and copper are the main components. The stream has a density of 1.16 g cm^{-3}, a free acidity of 7% and a pH of ~ 1.0.

The chelating resin used for the recovery of nickel and copper was Puromet™ MTS9600 functionalized with bis-picolylamine group (Bis-PMA). This resin forms coordinate bonds with most of the toxic metal ions via Lewis acid-base interactions. The main characteristics of the resin are summarized in Table 2.

The adsorption of metals with chelating resins is strongly dependent on the pH of the solution. For this reason, in order to adjust the pH of the effluent to be treated, H_2SO_4 95–98% and NaOH 5.0 M solutions, both supplied by Panreac, were employed. H_2SO_4 was also used in the desorption step together with NH_4OH 30–32% solution, supplied by Sigma Aldrich. The rinsing of the resin after desorption and protonation stages was performed with double deionized water (18 MΩ cm, MilliQ, Millipore).

2.2. Columns experiments

Fig. 1 shows a scheme of the process configuration used for the recovery of copper and nickel from the real spent acid effluent using two in-series fixed-bed columns. Column 1 is fed with the untreated spent acid in order to perform the recovery of copper over nickel, since at pH values below 1.0, the removal of nickel can be considered negligible, as demonstrated in previous works [8]. Column 2 is fed with the effluent of column 1 after an in-line pH adjustment to a value of 2.0, thus favoring nickel adsorption and avoiding iron precipitation (pH>3.0). After the loading stage, column 1 is regenerated with a 2.0 M NH_4OH solution and column 2 is treated with a 2.0 M H_2SO_4 solution, thus allowing the selective and independent recovery of both metals as was previously concluded in previous research [9]. The columns used have an effective length of 0.19 m and an inner diameter of 0.03 m, thus the bed volume is $1.3{\cdot}10^{-4}$ m^3. The void of the fixed column was calculated through the correlation proposed by Ribeiro and coworkers [40], which determines this parameter as a function of the column diameter and the resin particle diameter, obtaining a value of ε_B=0.38 (dimensionless). In order to avoid the generation of preferential pathways within the fixed-bed, glass fiber and glass spheres of 4.0 mm diameter are placed at both ends of the column. To complete the experimental system three tanks are also required, one for the storage of the feed solution to be treated, with a total capacity of 5.0 L (Feed Tank), and two of 2 L placed at the outlet of each column to collect the treated effluent, one called Accumulation

Table 1
Metals and ions concentrations of sulfuric-basic acid effluent.

[mg L^{-1}]	Al^{3+}	Cr^{3+}	Mn^{2+}	Ni^{2+}	Cu^{2+}	Zn^{2+}	Cd^{2+}	Sn^{2+}	Sb^{3+}	Pb^{2+}	Fe^{2+}	SO_4^{2-}
	544	380	64	8790	3367	384	<10	<10	306	59	24450	159300

Table 2
Physico-chemical characterization of the chelating resin Puromet™ MTS9600 [39].

Parameter	Value
Polymeric structure	Macroporous polystyrene cross-linked with divinylbenzene
Appearance	Spheres
Functional group	Bispicolylamine
Ionic shape	H^+
Maximum copper uptake capacity	35 g L^{-1}
Maximum nickel uptake capacity	25 g L^{-1}
Particle size	425 – 1000 μm
Particle density	750 – 800 g L^{-1}
Pore size	Macroporous (>50 nm)

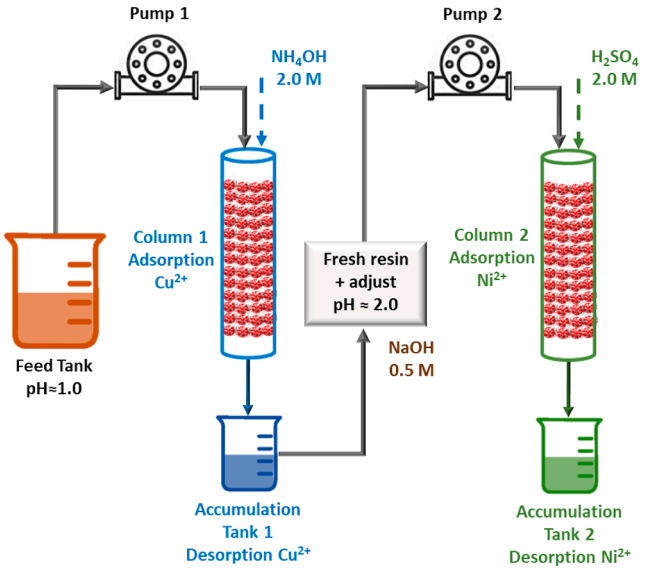

Fig. 1. Scheme of the adsorption / desorption treatment proposed in this study.

Tank 1 (column 1, copper recovery) and other called Accumulation Tank 2 (column 2, nickel recovery). The feed solution is circulated through the columns in a downward mode with flowrates between $3.0{\cdot}10^{-4}$ and $9.0{\cdot}10^{-4}$ m^3 h^{-1} using peristaltic pumps operating in the range between 4 and 105 mL min^{-1} (Fluid density (kg m^{-3}), ρ_F=1100; Fluid viscosity (kg m^{-1} h^{-1}), μ_F=3.6. Finally, a top to bottom flow configuration was selected as was recommended in the literature to keep stable flow conditions when low flowrates are employed [41,42]. Samples at different operation times were taken from the accumulation Tanks 1 and 2 and were stored until their analysis. The concentration of metal ions in each sample of the aqueous phase was measured by Microwave Plasma-Atomic Emission Spectrometry (MP-AES, Agilent, Spain). All experiments were carried out ambient temperature, 20 °C.

After describing the experimental performance of the adsorption and desorption steps, the theoretical analysis of the separation processes was carried out using the mathematical model described in Section 3, and the simulation software Aspen Custom Modeler V.12. The mathematical model was validated in order to obtain the model parameters that provide the minimum deviation between experimental and simulated data using the estimation tool of the Aspen software, following the least squared error criteria, with a maximum of 1150 iterations and a solution convergence tolerance of 0.0001.

3. Approach to the modeling of adsorption–desorption process

In general, the mathematical model describing the breakthrough curves in adsorption–desorption processes should consider the following general equations: i) mass balances to the target compounds in the fixed-bed column, ii) the description of the interfacial interaction between the solid and the target compounds described by either equilibrium or kinetic approaches, and iii) a set of equations describing internal and external mass transfer around the particle.

3.1. Modeling of copper and nickel adsorption–desorption in fixed-bed

Based on the experimental results reached by Ulloa and co-workers [8,9], it was concluded that: i) the adsorption equilibriums of copper and nickel with the resin Puromet™MTS9600 are described by the Langmuir and Freundlich models, respectively, ii) the dispersion term is included in the mass balance of the mathematical model due to the low operating flowrates (manufacturer's operating range and operation at high residence times), and iii) diffusion in the liquid film should be considered as a mass transfer controlling stage due to the low Reynolds numbers observed in the column. Considering these assumptions, the process has been modeled as a simplified intraparticle model (LDF), since it represents the desired concept in a simple and adequate way. The equations that constitute the mathematical model of adsorption/desorption of copper and nickel with the Puromet™ MTS9600 resin are shown below:

- Mass balances in the fixed bed column.

$$\varepsilon_B\frac{\partial C_i}{\partial t}+(\rho_P(1-\varepsilon_B)+\rho_F\varepsilon_B)10^{-3}\frac{\partial q_i}{\partial t}+\nu_F\frac{\partial C_i}{\partial t}-D_{ax,i}\varepsilon_B\frac{\partial^2 C_i}{\partial z^2}=0$$

$$\begin{aligned} &q_i=0 \quad C_i=0 \quad \text{for} \quad t=0\\ &C_i=C_{i,in} \quad \text{for} \quad z=0\\ &\frac{\partial C_i}{\partial z}=0 \quad \text{for} \quad z=L \end{aligned} \tag{1}$$

where C_i is the adsorbate (Cu^{2+} or Ni^{2+}) concentration in mg L^{-1}, q_i is the amount of adsorbate on the solid (intraparticle Cu^{2+} or Ni^{2+}) in mg kg dry $resin^{-1}$, ν_F is the velocity in m h^{-1}, $D_{ax,i}$ is the copper or nickel axial dispersion coefficient in m^2 h^{-1}. 10^{-3} is a factor used to make dimensions homogeneous.

- Diffusion in the external liquid film.

External diffusion can be analyzed with Boyd's equation as follows:

$$\begin{aligned} &(\rho_P(1-\varepsilon_B)+\rho_F\varepsilon_B)10^{-3}\frac{\partial q_i}{\partial t}=\pm k_L A_P(C_i-C_{i,eq})\\ &q_i=0 \quad \text{for} \quad t=0 \end{aligned} \tag{2}$$

where ρ_P is the density of the particle in kg m^{-3}, ρ_F is the density of the fluid in kg m^{-3}, k_L is the mass transfer coefficient in the liquid film in m h^{-1}, Ap is the external surface area per unit volume of the particle in m^2 m^{-3} and $C_{i,eq}$ is the adsorbate concentration in equilibrium with the solid in mg L^{-1}.

- Intraparticle diffusion.

Intraparticle mass transport can be associated with diffusional control (Eq. (3)) or with reaction rate control (Eq. (4)) as a controlling stage:

$$\frac{\partial q_i}{\partial t} = k_S\left(q_i - q_{i,eq}\right) \qquad q_i = 0 \quad \text{for} \quad t = 0 \tag{3}$$

where k_S is the intraparticle mass transfer coefficient (h^{-1}) and $q_{i,eq}$ is the copper concentration at equilibrium in the solid.

$$(\rho_P(1-\varepsilon_B) + \rho_F\varepsilon_B)10^{-3}\frac{\partial q_i}{\partial t} = k_{i,d}C_{i,eq}^{1/n} - k_{i,r}q_i$$

$$q_i = 0 \quad C_i = 0 \quad \text{for} \quad t = 0 \qquad q_i = q_{i,eq} \quad \text{for} \quad t = t_{eq} \tag{4}$$

where $k_{i,d}$ is the forward reaction rate ($(mg\ L^{-1})^{((n-1)/n)}\ h^{-1}$) and $k_{i,r}$ is the reverse reaction rate (kg dry resin $L^{-1}h^{-1}$), n and K_F=$k_{i,r}/k_{i,d}$ the parameter and the constant of the Freundlich equation (mg kg dry resin^{-1})(L mg^{-1})$^{1/n}$.

- Description of *adsorption/desorption equilibrium or kinetics*.

The adsorption equilibrium can be described by theoretical Langmuir and Freundlich isotherms in Eqs. (5) and (6):

$$q_{i,eq} = \frac{q_m K_{Lg} C_{i,eq}}{1 + K_{Lg}C_{i,eq}} \tag{5}$$

$$q_{i,eq} = K_{Fr}C_{i,e}^{1/n} \tag{6}$$

where q_m is the maximum adsorption capacity of the solid (mg kg dry resin^{-1}), $C_{i,eq}$ is the adsorbate concentration at equilibrium in the aqueous phase, K_{Lg} the constant of the Langmuir equation (L mg^{-1}), K_{Fr} (mg kg $kg_{dry\ resin}^{-1}$)(L mg^{-1})$^{1/n}$ are the Langmuir and Freundlich adsorption constants related to the bonding energy, respectively, and 1/n is an empirical Freundlich constant related to the heterogeneous nature of the adsorbent surface from an energetic point of view.

It is considered that, under the desorption operating conditions, the reaction only occurs in one direction, meaning that the desorbed ions are not re-adsorbed into the resin, and thus, the reaction can be described by a first order kinetic, modeled by equation (7).

$$(\rho_P(1-\varepsilon_B) + \rho_F\varepsilon_B)10^{-3}\frac{\partial q_i}{\partial t} = -k_{de,i}q_i$$

$$q_i = 0 \quad \text{for} \quad t = 0 \tag{7}$$

Where $k_{de,i}$ is the reaction rate in kg dry resin $L^{-1}\ h^{-1}$.

3.2. Calculation of model parameters

The axial dispersion coefficient is calculated through the correlation proposed by Levenspiel [43]:

$$D_{ax,i} = \frac{1.8\ \nu_F d_P}{\varepsilon_B} \tag{8}$$

where d_P is the particle diameter in m.

The external surface area per unit volume of the particle, A_P is obtained from the following equation:

$$A_P = \frac{6}{d_P} \tag{9}$$

The mass transfer coefficient in the liquid phase is calculated through the correlation proposed by Wilson and Geankopolis, relative to the Sherwood number (Sh) as a function of the dimensionless numbers of Reynolds (Re) and Schmidt (Sc) [44]:

$$Sh = \frac{1.09}{\varepsilon_B}Re^{1/3}Sc^{1/3} \tag{10}$$

This expression is valid in the ranges 0.0016<Re<55 and 165<Sc<70600, which are within the operating ranges of the system [45], being:

$$Re = \frac{\rho_F \nu_F d_p}{\mu_F} \qquad Sc = \frac{\mu_F}{\rho_F D_{m,i}} \qquad Sh = \frac{k_L}{d_p D_{m,i}} \tag{11}$$

where μ is the viscosity of the fluid in kg m^{-1} h^{-1}, $D_{m,i}$ is the coefficient of molecular diffusion of copper or nickel, in m h^{-1}, which is calculated using the Worch equation [36]:

$$D_{m,i} = \frac{3.595 \times 10^{-14}T}{\mu_F M_i^{0,53}} \tag{12}$$

where M_i is the molecular weight in g mol^{-1} and T is the temperature in K.

The mass transfer coefficient intraparticle or in the solid is calculated from the following correlation [46]:

$$k_{S,ds} = \frac{5A_P\ D_s}{r_p} \tag{13}$$

where D_S is the diffusion coefficient of the solid in m^2 h^{-1} and r_p is the particle radius in m.

3.3. Mass balances in the batch stirred tank

For each column-tank system, as seen in Fig. 1, the fixed-bed outlet concentration is accumulated in a perfect mixed tank to facilitate the collection of samples and the analysis of copper and nickel concentrations:

$$Q_i\ C_{i,in}^T = \frac{d\left(V_i^T C_i^T\right)}{dt} = \frac{dV_i^T}{dt}C_i^T + \frac{dC_i^T}{dt}V_i^T \tag{14}$$

Where $C_{i,in}^T$ (mg L^{-1}) is the initial concentration in the tank, Ci^T (mg L^{-1}) is the concentration in the tank, Q_i is the working flow rate for each adsorbate (m^3 h^{-1}) and V_i^T (L) is the volume of the stirred tank (copper tank, nickel tank, Fig. 1) which is continuously increasing:

$$\frac{dV_i^T}{dt} = Q_i \qquad C_{i,out}^T(\text{ para } t = t\ y\ z = L) = C_{i,in}^T \quad \text{for} \quad t = 0 \tag{15}$$

4. Results and discussion

4.1. Adsorption-desorption kinetics of Ni^{2+}/Cu^{2+} in fixed-bed columns

4.1.1. Experimental results

The adsorption kinetics of nickel and copper were studied in the continuous process shown in Fig. 1, with the effluent characterized in Table 1 and the chelating resin characterized in Table 2. This industrial effluent, without any pH modification, flowed through columns 1 and 2, as it is shown in Fig. 1. The dimensionless breakthrough curves obtained for copper, nickel and iron measured in Tank 1, are depicted in Fig. 2. As reported in previous works [9], when working pH values were below 2.0, the adsorption of nickel and iron is not favored, while copper removal is very effective. Nickel and iron breakthrough curves show asymptotic behavior after one hour of operation, with concentration values leaving column 1 around 8000 mg L^{-1} and 21600 mg L^{-1}, respectively (90–100% of the inlet concentration, depending on whether a new resin or a regenerated one is used). In the case of copper, the measured concentration is negligible during the first two operating hours. At this point, the concentration measured in the accumulation Tank 1 starts rising, due to the saturation of the column 1. Copper concentration increases until reaching the asymptotic behavior after twenty hours of treatment, with values around 2100 mg L^{-1} (80% of the feed concentration). The concentration of copper inside the column 1 reached a constant value of 45000 mg Cu^{2+} per kg of dry resin after five hours of treatment. This value agrees with the equilibrium value

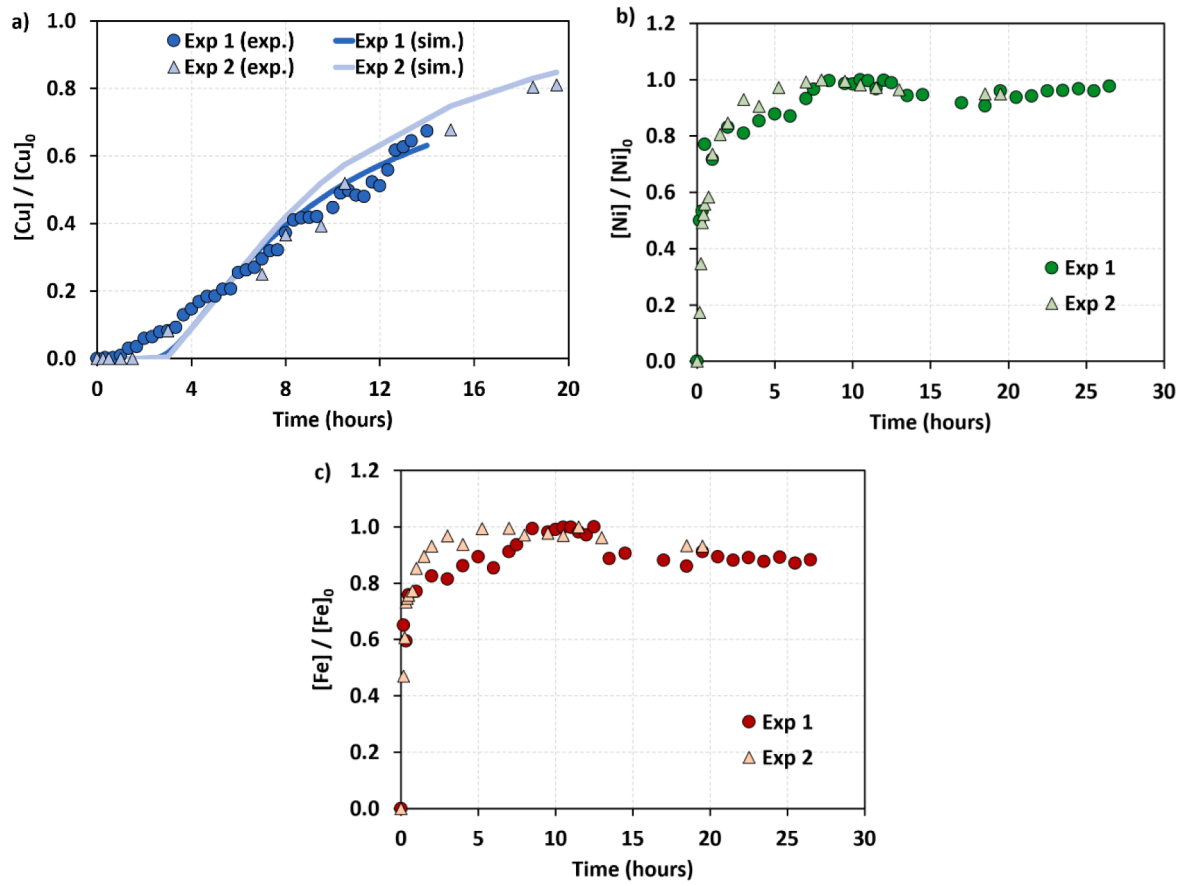

Fig. 2. Dimensionless adsorption breakthrough curves for a) copper, b) nickel and c) iron in Tank 1.

calculated by Ulloa and co-workers for the system copper-Puromet MTS9600 [9], which predicts a load inside the column of around 48000 mg Cu^{2+} per kg of dry resin for concentrations in the liquid phase in the range of 2600 mg L^{-1}.

After treatment in column 1, the effluent is contacted with an excess of fresh resin in order to remove the remaining amount of copper, and the pH is adjusted to a value of 2.0 with NaOH 5.0 M, in order to set up the optimized conditions to perform the selective recovery of nickel to its way through column 2. Fig. 3 shows the dimensionless breakthrough curves for nickel and iron obtained in Tank 2, where it is assumed that copper inflowing this column 2 is negligible.

Under these operating conditions, the separation of nickel is favored, while the removal of iron is negligible, as observed in Fig. 3. Iron dimensionless concentration shows an asymptotic behavior after the first hour of operation, with a measured output concentration of 18300 mg L^{-1}, which represents 85% of the input concentration. For nickel, the asymptotic behavior is reached after eight hours of treatment, time lower than the time required in the case of copper in column 1. It is also noted that, in contrast with copper, the accumulation Tank 2 nickel concentration increases since the beginning of the treatment, due to the faster saturation of the column 2. These factors support the evidence that, although the chelating resin has a high affinity for nickel, it preferentially adsorbs copper even under the most unfavorable conditions. The concentration of nickel inside the column 2 can be considered constant after five operating hours, with a value of 32000 mg Ni^{2+} per kg of dry resin. This value also agrees with the equilibrium value

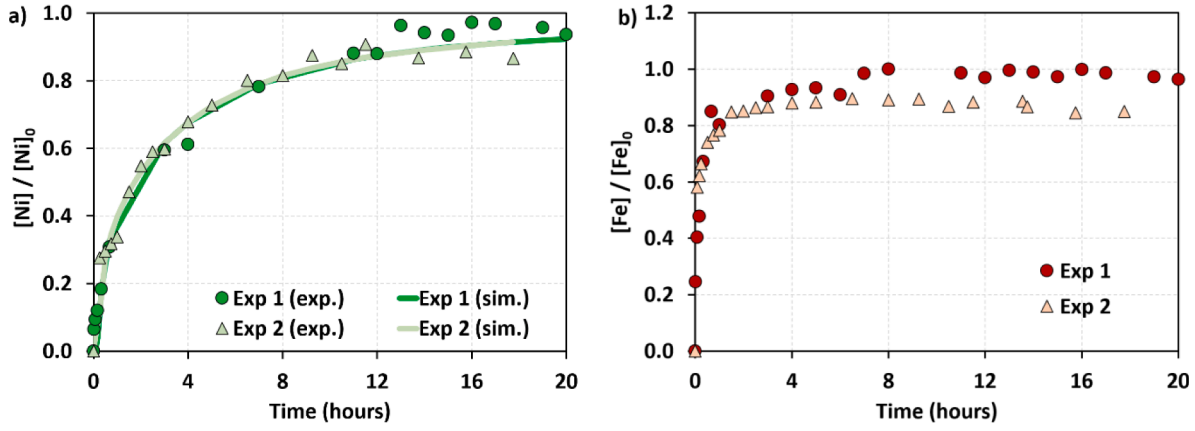

Fig. 3. Dimensionless adsorption breakthrough curves for a) nickel and b) iron in Tank 2.

calculated by Ulloa and co-workers [9], which is expected to be 34000 mg Ni^{2+} per kg of dry resin for concentrations in the liquid phase inside the column 2 around 9000 mg L^{-1}. The results obtained from the nickel adsorption process indicate that, under the selected operating conditions, the saturation of the column 2 happens too fast. This might be due to the elevated ratio between the load of nickel in the input stream and the load of resin inside the column 2. Increasing the length of the column, and thus, the amount of resin that it contains, may result in a better nickel adsorption performance. Published studies about the simultaneous recovery of nickel and copper, from synthetic multicomponent mixtures, obtained similar adsorption breakthrough curves. Perez and coworkers [28] removed some metal ions, including Ni^{2+} and Cu^{2+}, from synthetic solutions, which simulate the waste product from the hydrometallurgical processing of nickel laterite ores using Dowex XUS 43605 chelating resin with HPPA functional group. The adsorption breakthrough curve of copper and nickel has a similar shape to the one obtained in this study, with copper reaching the saturation point later than nickel and with a lower slope curve. Viniza and coworkers [47], using the Dowex M−4195 resin functionalized with bis(2-pyridylmethyl) amine groups, and Riley and coworkers [48] using the Dowex M4195 resin functionalized with bis-picolylamine groups at low pH values, obtaining adsorption breakthrough curves that suggest that the adsorption of copper is favored over the adsorption of nickel.

Although a small amount of nickel and iron is adsorbed in column 1 and a small amount of iron is adsorbed in column 2, those quantities can be considered negligible in comparison with the values of copper and nickel loaded inside each column. The desorption process is then carried out in order to recover copper and nickel selectively from their respective columns. The selection of the desorption agents for copper-Puromet MTS9600 and nickel-Puromet MTS9600 systems and the optimal operating conditions was performed by Ulloa and co-workers in previous work [9]. Based on the conclusions of this work, the regeneration of column 1 was carried out with a solution of NH_4OH 2.0 M with a flowrate between $3.0{\cdot}10^{-4}$-$9.0{\cdot}10^{-4}$ $m^3\,h^{-1}$, collecting the effluent in an accumulation Tank 1, in which the evolution of copper concentration was measured. Column 2 was treated with a solution of H_2SO_4 2.0 M, with flowrates between $3.0{\cdot}10^{-4}$-$5.0{\cdot}10^{-4}$ $m^3\,h^{-1}$ and the effluent was collected in a separate accumulation Tank 2 in order to measure the evolution of the output nickel concentration. The desorption breakthrough curves for copper and nickel obtained in their respective tanks during the experiments are shown in Fig. 4.

Fig. 4 shows that the desorption process of copper and nickel have similar behavior. For both columns the desorption process exhibited faster kinetics than the adsorption one, reaching an asymptotic behavior after four operating hours. The high concentration increase at the beginning of the desorption, associated with an elevated amount of copper and nickel leaving the columns, shows that under the selected conditions the desorption of both metals is favored. The peak concentration in the tank is reached after one hour of treatment. After this point, the concentration decreases as the effluents leaving the columns have a lower metal load. The concentration of copper and nickel inside the column reaches constant values after two operating hours (5000 mg Cu^{2+} per kg of dry resin and 6000 mg Ni^{2+} per kg of dry resin), which means that 90% of copper and about 80% of nickel have been released during the desorption stage. In order to valorize the copper and nickel streams obtained after desorption, nowadays, it is being evaluated to apply an electrodeposition process, in order to obtain metallic nickel and copper from these solutions, as shown in previous studies such as Carrillo-Abad and coworkers performed electrodeposition of divalent metal ions present in low pH solutions obtaining promising results [49], and Al-Murshedi and coworkers evaluated the electrodeposition of nickel and copper ions dissolved in different media with positive results [50]. Taking to account the literature, electrodeposition can be as a suitable strategy for the further valorization of the metals recovered during the proposed adsorption–desorption process. Finally, since the hazardous character of the initial solution was associated with the presence of nickel, and this nickel is almost completely removed during the adsorption in column 2, it is considered that the effluent leaving the system can be managed as a non-hazardous waste in an ordinary landfill, considerably decreasing its management costs and environmental impact or it can be employed as a secondary source of iron, i.e. development of coagulation agents [51,52].

4.1.2. Simulation analysis

The mathematical model described in section 3 of this work is implemented and validated using the experimental results depicted and discussed in section 4.1.1. For this purpose, the models were solved using the commercial software package Aspen Custom Modeler V.12 (AspenTech).

The adsorption of copper in column 1 can be described with Eq. (1) to (4), while the equilibrium follows a Langmuir model represented by equation (5). The dimensionless numbers, parameters and mass transfer coefficients needed to apply the model are calculated using Eq. (8) to (13). Finally, the behavior of the accumulation Tank 1 is modeled with Eq. (14) and (15). For nickel, the adsorption process in the column 2 can be described by the same set of equations as copper, but, in this case, the adsorption equilibrium is described by means of a Freundlich Isotherm (Eq. (6)). Langmuir's and Freundlich's parameters required to describe the adsorption thermodynamics of copper and nickel were determined in a previous work, respectively [8]. For nickel, the behavior of the accumulation Tank 2 is modeled with Eq. (14) and (15). Table 3 shows the values of the main parameters used to describe the adsorption process for both metals.

The mathematical model used for the simulation of the adsorption process can also be used to simulate the desorption of copper and nickel, but considering several assumptions. As it was discussed in section

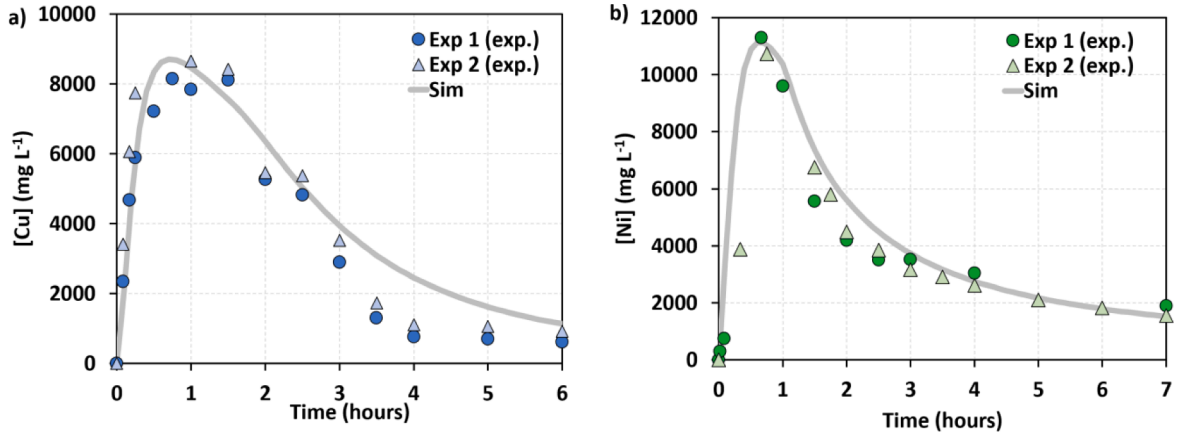

Fig. 4. Desorption breakthrough curves for a) copper in Tank 1 and b) nickel in Tank 2.

Table 3
Model parameters for adsorption process for both metals.

Parameter	Copper	Nickel
D_{ax} (m h^{-2})	$1.16{\cdot}10^{-3}$	$1.23{\cdot}10^{-3}$
D_m (m h^{-1})	$4.20{\cdot}10^{-6}$	$4.38{\cdot}10^{-6}$
k_s (m h^{-1})	$1.18{\cdot}10^{-1}$	
k_L (m h^{-1})	$9.39{\cdot}10^{-4}$	$3.23{\cdot}10^{-4}$
K_{Lg} (L mg^{-1}) [8]	$9.10{\cdot}10^{-2} \pm$	
q_m (mg $Kg^{-1}_{dry\ resin}$) [8]	$5.00{\cdot}10^{-3}$	
	48309 ± 2657	
K_{Fr} (mg Kg dry $resin^{-1}$ (L $mg^{-1})^{1/n}$)		645 ± 38
1/n (-) [8]		$4.36{\cdot}10^{-1} \pm$
		$2.60{\cdot}10^{-2}$

4.1.1., the desorption of both metals is faster than their adsorption. This difference can be associated with a difference in the microscopic phenomena involved in adsorption and desorption stages. In the case of desorption, it is assumed that the release of both metals from the resin can be described as a first order kinetic model, described by equation (7). The values of the kinetic constants for both metals were estimated from the experimental results using Aspen Custom Modeler with a minimal squared error criterion. The rest of the parameters required to solve the model were calculated using the same equations as those used to describe the adsorption, but adjusting the operating conditions where appropriate. Table 4 shows the values of the main parameters used to describe the desorption process for both metals.

The models were validated using the experimental data previously reported in Section 4.1.1. Fig. 2 a) and 3 a) show the fitting between the simulated values of copper and nickel in their respective accumulation tanks and the corresponding experimental results. Fig. 4 shows the fit between experimental and simulated data for the desorption of both copper and nickel.

The deviation between both data sets is quantified by the parity graphs shown in Fig. 5 and the R-squared parameter (R^2) defined as follows.

$$R^2 = 1 - \frac{\sum \left(C_{exp,i} - C_{sim,i}\right)^2}{\sum \left(C_{exp,i} - \overline{C_{exp}}\right)^2} \quad (16)$$

It is concluded that, for the adsorption, 82% of simulated copper concentrations in the accumulation tank fall within the range $[Cu]_{EXP}$±20%$[Cu]_{EXP}$, with values of R^2 between 0.96 and 0.97. On the other hand, 90% of the simulated data of nickel concentrations fall within the range $[Ni]_{EXP}$±20%$[Ni]_{EXP}$, with values of R^2 between 0.98 and 0.99. In the case of desorption, 75% of simulated copper concentrations in the accumulation tank fall within the range $[Cu]_{EXP}$±20% $[Cu]_{EXP}$, with values of R^2 about 0.91. On the other hand, 60% of the simulated data of nickel concentrations fall within the range $[Ni]_{EXP}$±20%$[Ni]_{EXP}$, with R^2 values around 0.90.

From these results, it is concluded that, in general, the model allows a more accurate representation of the adsorption process, but, considering the complex nature of the treated solutions and the involved processes, it is thought that the proposed model permits a satisfactory description of the system. Thus, it is therefore possible to use this model for future predictions and for the scaling up of the process.

Table 4
Model parameters for desorption.

Parameter	Copper	Nickel
D_{ax} (m h^{-2})	$5.78{\cdot}10^{-3}$	$1.1{\cdot}10^{-3}$
D_m (m h^{-1})	$4.20{\cdot}10^{-6}$	$4.38{\cdot}10^{-6}$
k_s (m h^{-1})	$3.75{\cdot}10^{-1}$	$6.05{\cdot}10^{-2}$
k_{de} (kg dry resin $L^{-1}h^{-1}$)	0.81	1.10

5. Simulation analysis

5.1. Influence of column sizing on the adsorption kinetics

The mathematical model developed in section 2 and validated in section 4.1 is a useful tool to predict the behavior of the system under different operating scales and conditions. As it was mentioned above, one of the major problems of the separation is the rapid saturation of column 2 during nickel adsorption, due to the small amount of resin used in the experiments. Although the experimental results are useful for the model validation, the adsorption of nickel has been simulated using different amounts of resin inside the column in order to evaluate the influence of process sizing on the evolution of the breakthrough adsorption curves. All simulations were performed considering a nickel input concentration of 7975 mg L^{-1} and a constant flow rate of $3.4{\cdot}10^{-4}$ m^3 h^{-1} and resin loads varying in the range between 0.1 kg and 1.5 kg. Fig. 6 shows the nickel breakthrough at the exit of the column 2.

As can be observed in Fig. 6, as the column size increases (greater amount of resin available for the adsorption), the effective operating time before reaching the saturation of the column is longer. When the amount of resin inside the column is 0.4 Kg, the shape of the breakthrough curve for nickel is similar to the one obtained for copper at the outlet of column one containing 0.1 kg of resin (Fig. 7). These results are consistent with the differences in the initial values of concentration of nickel and copper in the spent solution where the initial molar ratio Ni^{2+}/Cu^{2+} is 3.60.

By simulating a resin mass ratio between column 2 and column 1 of 4.0, slightly higher than the molar ratio between nickel and copper at the input, it is observed that the saturation of column 2 (nickel) is faster than that of column 1 (copper), which causes the increase of the nickel output concentration at shorter operation times. These results are consistent with the conclusions reached in previous works, which indicate that the adsorption of copper is favored even under the most not favorable operating conditions.

5.2. Influence of resin deactivation on the adsorption kinetics

In general, adsorption processes might be affected by the deactivation of the resin for several reasons such as chemical modification caused by contact with the feed solution, dragging by the fluid flow, partial efficiency of the regeneration steps, etc. In this way, the mathematical model has been employed to evaluate the adsorption kinetics when several cycles of adsorption–desorption were performed and the resin loses efficiency during the operation. In particular, Fig. 8 shows different adsorption breakthrough curves of copper obtained at the exit of the fixed-bed column (out) containing 0.1 kg of fresh resin and assuming that after each adsorption–desorption cycle the initial load of copper on the resin surface increases 15%. All simulations were performed with copper inlet concentration of 2397 mg L^{-1} and a constant flowrate of $3.4{\cdot}10^{-4}$ m^3 h^{-1}. The results obtained are shown in Fig. 8.

From the results depicted in Fig. 8, it is concluded that the increase in the initial concentration of copper in the resin, strongly affects the kinetics of adsorption. In the first cycle using fresh resin, the concentration of copper starts rising after 4 h of operation; on the other hand, in the fourth cycle that employs a resin with an initial concentration of copper of around 22000 mg per Kg of dry resin, the step in the breakthrough curve is detected after the first hour of operation. This prediction will be useful in future stages of the scaling up of the process in order to select the optimum operating conditions for the adsorption and desorption cycles.

6. Conclusions

This work reports on the selective recovery of nickel and copper from a spent acid solution provided by a local waste management company, whose main components are copper (34000 mg L^{-1}), nickel (8700 mg L^{-1}) and iron (24000 mg L^{-1}). For this, it was analyzed the

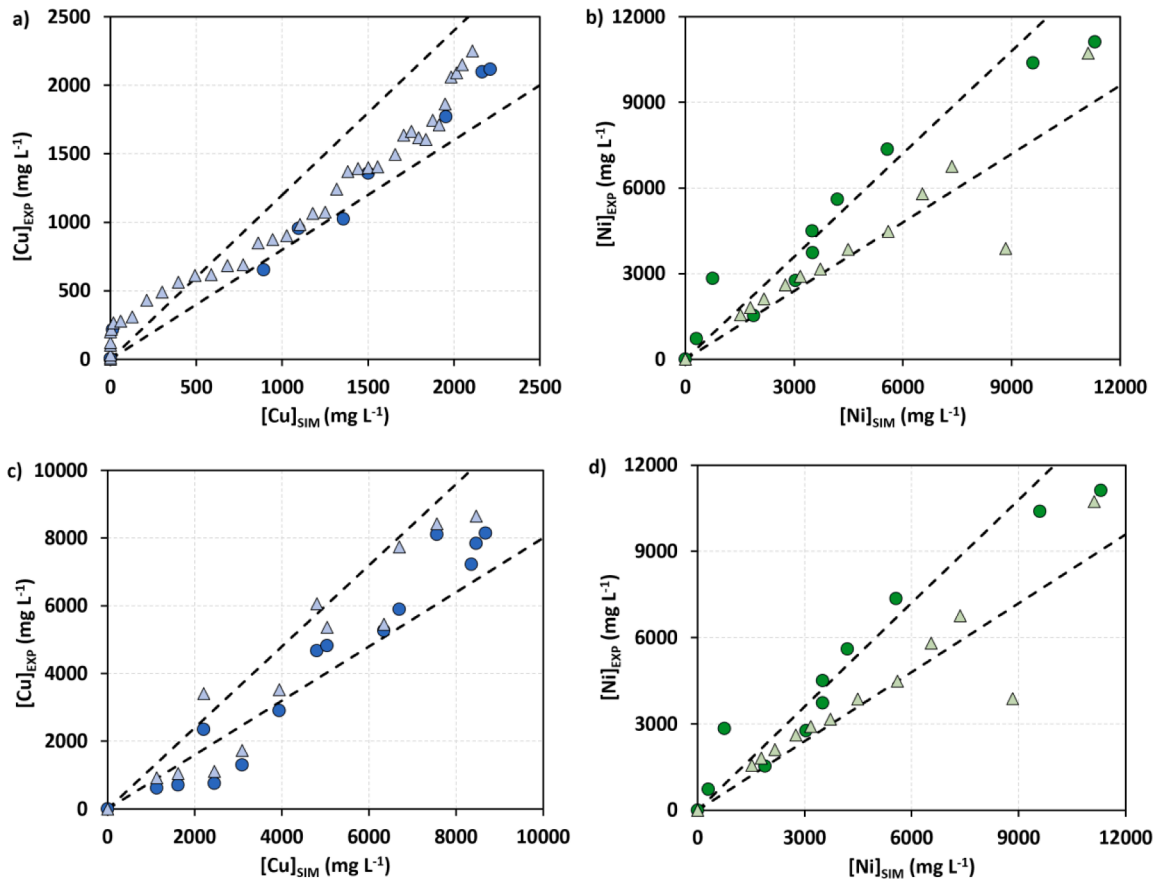

Fig. 5. Parity graphs. Comparison of experimental (EXP) and predicted (SIM) values of concentration in the accumulation tank of a) copper adsorption, b) nickel adsorption, c) copper desorption and d) nickel desorption.

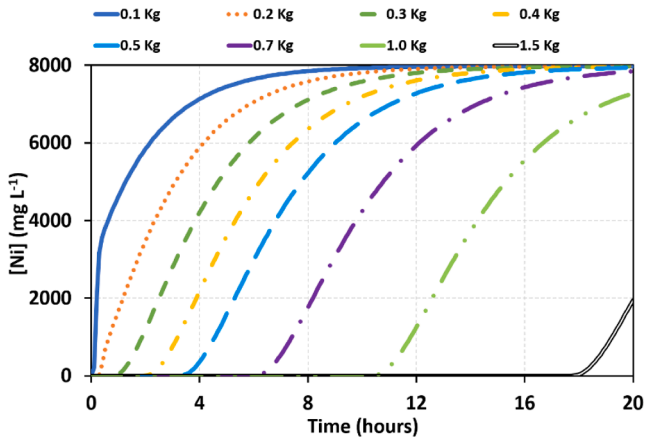

Fig. 6. Nickel simulated rupture curves loaded with different amounts of resin (output from column 2).

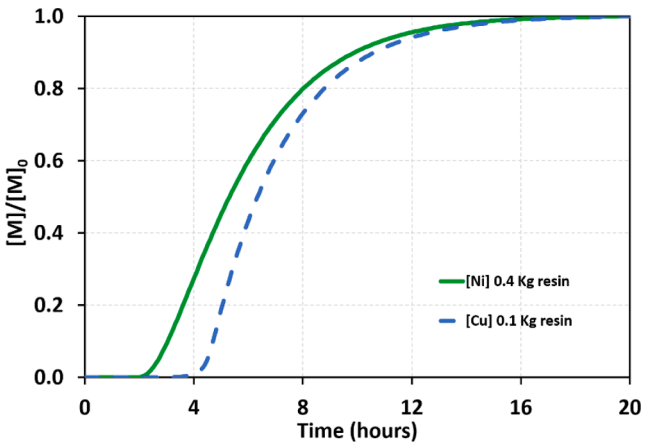

Fig. 7. Influence of column sizing on nickel and copper adsorption kinetics.

selective adsorption and desorption of both metals using the chelating resin Puromet MTS9600 in a continuous operating mode. From the experimental results, it is concluded that, under the selected operating conditions, it is possible to recover 90% of copper and 80% of nickel present in the problem solution. The selected resin shows a better affinity for copper, leading to a better performance in the adsorption stage, although the desorption process shows a similar behavior for both metals.

The mathematical model proposed to describe the adsorption–desorption process consists of a system of differential and algebraic equations corresponding to the mass balances of copper and nickel in the ion exchange columns and the accumulation tanks as well as the mass transfer equations through the liquid and solid phases inside the column and the adsorption–desorption reactions. In the case of adsorption, the chemical reactions were modeled as equilibrium reactions, fitting to Langmuir's and Freundlich's isotherms for copper and nickel respectively. In the case of desorption, the chemical reactions for both metals fit into first order reactions, whose kinetic constants were estimated using the commercial software Aspen Custom modeler, obtaining a value of k_{de}=0.81 $kg_{dryresin}$ L^{-1} h^{-1} for copper and k_{de}=1.10 $kg_{dryresin}$ L^{-1} h^{-1} for nickel. Predicted values agreed satisfactory well to the experimental data.

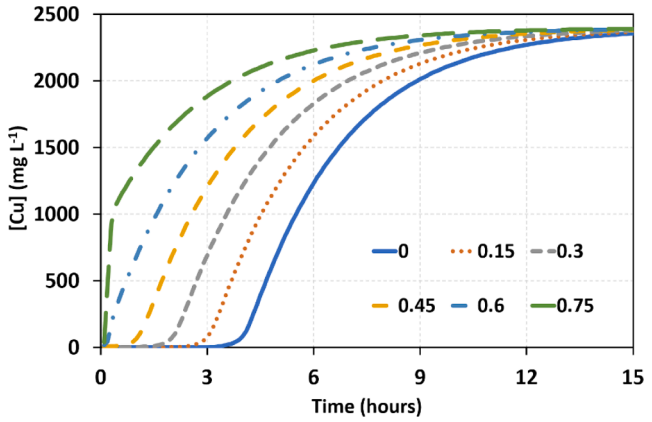

Fig. 8. Influence of the resin deactivation on the adsorption kinetics of copper.

CRediT authorship contribution statement

A. Bringas: Formal analysis, Software, Writing – original draft. **E. Bringas:** Investigation, Conceptualization, Methodology, Software, Formal analysis, Writing – review & editing. **R. Ibañez:** Funding acquisition. **Ma-F. San-Román:** Investigation, Conceptualization, Methodology, Software, Formal analysis, Writing – review & editing, Supervision, Funding acquisition.

Declaration of Competing Interest

The authors declare that they have no known competing financial interests or personal relationships that could have appeared to influence the work reported in this paper.

Data availability

The data that has been used is confidential.

Acknowledgements

This research was developed in the framework of the projects PID2020-115409RB-I00, PDC2021-120786-I00, TED2021-129874B-I00 and PID2021-122563OB-I00 financed by the Ministry of Science and Innovation (Spain).

References

[1] THE 17 GOALS | Sustainable Development https://sdgs.un.org/goals, 2022 (accessed October 10, 2022).
[2] E. Cerdá, A. Khalilova, Economía Circular, estrategia y competitividad empresarial, Economía Industrial. 401 (2016) 11–20.
[3] V. Prieto-Sandoval, C. Jaca, M. Ormazabal, Economía Circular: relación con la evolución del concepto de sostenibilidad y estrategias para su implementación, Memoria Investigaciones en Ingeniería. 15 (2017) 85–95.
[4] How to Build a Circular Economy, Ellen MacArthur Foundation. https://ellenmacarthurfoundation.org/, 2022 (accessed October 10, 2022).
[5] R.M. Machado, M.L.F. Gameiro, M. Krupa, J.M.A. Rodrigues, M.R.C. Ismael, M.T. A. Reis, J.M.R. Carvalho, Selective separation and recovery of zinc and lead from galvanizing industrial effluents by anion exchange, Sep. Sci. Technol. 50 (2015) 2726–2736, https://doi.org/10.1080/01496395.2015.1062029.
[6] C. Frías, O. Pérez, Recuperación de ácidos y metales en baños agotados del decapado de aceros inoxidables, Rev. Metal Madrid. 786 (1998) 427–431, https://doi.org/10.3989/revmetalm.1998.v34.iExtra.786.
[7] G. Leonzio, Recovery of metal sulphates and hydrochloric acid from spent pickling liquors, J Clean Prod. 129 (2016) 417–426, https://doi.org/10.1016/j.jclepro.2016.04.037.
[8] L. Ulloa, E. Bringas, M.F. San-Román, Simultaneous separation of nickel and copper from sulfuric acid, J. Chem. Technol. Biotechnol. 95 (2020) 1906–1914, https://doi.org/10.1002/jctb.6364.
[9] L. Ulloa, M. Martínez-Minchero, E. Bringas, A. Cobo, M.F. San-Román, Split regeneration of chelating resins for the selective recovery of nickel and copper, Sep. Purif. Technol. 253 (2020) 117516, https://doi.org/10.1016/j.seppur.2020.117516.
[10] C. Hagelüken, J.U. Lee-Shin, A. Carpentier, C. Heron, The EU Circular Economy and its relevance to metal recycling, Recycling. 1 (2016) 242–253, https://doi.org/10.3390/recycling1020242.
[11] M. Martínez-Minchero, L. Ulloa, A. Cobo, E. Bringas, M.F. San-Román, J.M. López-Higuera, Laser-induced breakdown spectroscopy analysis of copper and nickel in chelating resins for metal recovery in wastewater, Spectrochim. Acta Part B At. Spectrosc. 180 (2021) 106170, https://doi.org/10.1016/j.sab.2021.106170.
[12] M.F. San Román, I. Ortiz Gándara, R. Ibañez, I. Ortiz, Hybrid membrane process for the recovery of major components (zinc, iron and HCl) from spent pickling effluents, J. Memb. Sci. 415–416 (2012) 616–623, https://doi.org/10.1016/j.memsci.2012.05.063.
[13] M.F. San Román, E. Bringas, R. Ibañez, I. Ortiz, Liquid membrane technology: fundamentals and review of its applications, J. Chem. Technol. Biotechnol. 85 (2010) 2–10, https://doi.org/10.1002/jctb.2252.
[14] K. Yan, P. Huang, M. Xia, X. Xie, L. Sun, W. Lei, F. Wang, An efficient Two-Chamber Electrodeposition-Electrodialysis combination craft for nickel recovery and phosphorus removal from spent electroless nickel plating bath, Sep. Purif. Technol. 295 (2022) 121283, https://doi.org/10.1016/j.seppur.2022.121283.
[15] S.S. Goh, M. Rafatullah, N. Ismail, M. Alam, M.R. Siddiqui, E.K. Seow, Separation of Chromium (VI), Copper and Zinc: Chemistry of Transport of Metal Ions across Supported Liquid Membrane, Membranes. 12 (2022) 685, https://doi.org/10.3390/membranes12070685.
[16] A. Pohl, Removal of heavy metal ions from water and wastewaters by sulfur-containing precipitation agents, Water Air Soil Pollut. 231 (2020) 503, https://doi.org/10.1007/s11270-020-04863-w.
[17] A.L. Bojic, D. Bojic, T. Andjelkovic, Removal of Cu^{2+} and Zn^{2+} from model wastewaters by spontaneous reduction–coagulation process in flow conditions, J. Hazard. Mater. 168 (2009) 813–819, https://doi.org/10.1016/j.jhazmat.2009.02.096.
[18] A. Bashir, L.A. Malik, S. Ahad, T. Manzoor, M.A. Bhat, G.N. Dar, A.H. Pandith, Removal of heavy metal ions from aqueous system by ion–exchange and biosorption methods, Environ. Chem. Lett. 17 (2019) 729–754, https://doi.org/10.1007/s10311-018-00828-y.
[19] D. Humelnicu, M.M. Lazar, M. Ignat, I.A. Dinu, E.S. Dragan, M.V. Dinu, Removal of heavy metal ions from multi-component aqueous solutions by eco-friendly and low-cost composite sorbents with anisotropic pores, J. Hazard. Mater. 381 (2020) 120980, https://doi.org/10.1016/j.jhazmat.2019.120980.
[20] T.R. Sethy, T. Biswal, P.K. Sahoo, An indigenous tool for the adsorption of rare earth metal ions from the spent magnet e-waste: An eco-friendly chitosan biopolymer nanocomposite hydrogel, Sep. Purif. Technol. 309 (2022) 121283, https://doi.org/10.1016/j.seppur.2022.122935.
[21] P.R. Yaashikaa, P. Senthil Kumar, V.P. Mohan Babu, R. Kanaka Durga, V. Manivasagan, K. Saranya, A. Saravanan, Modelling on the removal of Cr(VI) ions from aquatic system using mixed biosorbent *(Pseudomonas stutzeri* and acid treated Banyan tree bark), J. Mol. Liq. 276 (2019) 362–370, https://doi.org/10.1016/j.molliq.2018.12.004.
[22] M. Nazaripour, M.A.M. Reshadi, S.A. Mirbagheri, M. Nazaripour, A. Bazargan, Research trends of heavy metal removal from aqueous environments, J. Environ. Manage. 287 (2021) 112322, https://doi.org/10.1016/j.jenvman.2021.112322.
[23] D.C. Ong, S.B. Tumampos, C.C. Kan, S.M.B. Pingul-Ong, B.M.B. Ensano, M.D.G. de Luna, Optimization of manganese recovery from groundwater treatment sludge for the production of highly-efficient Cu(II) and Pb(II) adsorbents, J. Environ. Chem. Eng. 9 (2021) 104705, https://doi.org/10.1016/j.jece.2020.104705.
[24] A. Ortiz, I. Fernández-Olmo, A. Urtiaga, I. Ortiz, Modeling of Iron Removal from Spent Passivation Baths by Ion Exchange in Fixed-Bed Operation, Ind. Eng. Chem. Res. 48 (2009) 7448–7452, https://doi.org/10.1021/ie900407c.
[25] P. Swain, C. Mallika, R. Srinivasan, U.K. Mudali, R. Natarajan, Separation and recovery of ruthenium: a review, J. Radioanal. Nucl. Chem. 298 (2013) 781–796, https://doi.org/10.1007/s10967-013-2536-5.
[26] G. Chauhan, K.K. Pant, K.D.P. Nigam, Metal Recovery from Hydroprocessing Spent Catalyst: A Green Chemical Engineering Approach, Ind. Eng. Chem. Res. 52 (2013) 16724–16736, https://doi.org/10.1021/ie4024484.
[27] J. Jiang, X.S. Ma, L.Y. Xu, L.H. Wang, G.Y. Liu, Q.F. Xu, J.M. Lu, Y. Zhang, Applications of chelating resin for heavy metal removal from wastewater, e-Polymers. 15 (2015) 161–167, https://doi.org/10.1515/epoly-2014-0192.
[28] I.D. Perez, A.B. Botelho Junior, P. Aliprandini, D.C.R. Espinosa, D. Perez, Copper recovery from nickel laterite with high-iron content: A continuous process from mining waste, Can. J. Chem. Eng. 98 (2020) 957–968, https://doi.org/10.1002/cjce.23667.
[29] A. Deepatana, J.A. Tang, M. Valix, Comparative study of chelating ion exchange resins for metal recovery from bioleaching of nickel laterite ores, Miner. Eng. 19 (2006) 1280–1289, https://doi.org/10.1016/j.mineng.2006.04.015.
[30] M. Cegłowski, G. Schroeder, Preparation of porous resin with Schiff base chelating groups for removal of heavy metal ions from aqueous solutions, Chem. Eng. J. 263 (2015) 402–411, https://doi.org/10.1016/j.cej.2014.11.047.
[31] N.M. Marin, A. Fical, L.A. Constantin, L. Motelica, R. Trusca, New Chelate Resins Prepared with Direct Red 23 for Cd2+, Ni2+, Cu2+ and Pb2+ Removal, Polymers 14 (2022) 5523, https://doi.org/10.3390/polym14245523.
[32] G. Duan, X. Li, X. Ma, W. Zhong, S. Wang, High-efficiency adsorption removal for Cu(II) and Ni(II) using a novel acylamino dihydroxamic acid chelating resin, Sci. Total Environ. 864 (2023) 160984, https://doi.org/10.1016/j.scitotenv.2022.160984.
[33] A. Wolowicz, Z. Hubicki, The use of the chelating resin of a new generation Lewatit MonoPlus TP-220 with the bis-picolylamine functional groups in the removal of selected metal ions from acidic solutions, Chem. Eng. J. 197 (2012) 493–508, https://doi.org/10.1016/j.cej.2012.05.047.

[34] X. Lin, Q. Huang, G. Qi, S. Shi, L. Xiong, C. Huang, X. Chen, H. Li, X. Chen, Estimation of fixed-bed column parameters and mathematical modeling of breakthrough behaviors for adsorption of levulinic acid from aqueous solution using SY-01 resin, Sep. Purif. Technol. 174 (2017) 222–231, https://doi.org/10.1016/j.seppur.2016.10.016.

[35] M. Siahpoosh, S. Fatemi, A. Vatani, Mathematical modeling of single and multi-component adsorption fixed beds to rigorously predict the mass transfer zone and breakthrough curves, Iran J. Chem. Chem. Eng. 51 (2009) 25–44, https://doi.org/10.30492/IJCCE.2009.6844.

[36] E. Worch, Fixed-bed adsorption in drinking water treatment: a critical review on models and parameter estimation, J. Water Supply Res. T. 57 (2008) 171–183, https://doi.org/10.2166/aqua.2008.100.

[37] H. Naidu, A.P. Mathews, Linear driving force analysis of adsorption dynamics in stratified fixed bed adsorbers, Sep. Purif. Technol. 257 (2021) 117955, https://doi.org/10.1016/j.seppur.2020.117955.

[38] D. Fang, X. Zhuang, L. Huang, Q. Zhang, Q. Shen, L. Jiang, X. Xu, F. Ji, Developing the new kinetics model based on the adsorption process: From fitting to comparison and prediction, Sci. Total Environ. 725 (2020), 138490, https://doi.org/10.1016/j.scitotenv.2020.138490.

[39] Purolite - Puromet MTS9600. Data sheet Puromet MTS9600. https://www.purolite.com/product/es/mts9600 [27 January 2023].

[40] A.M. Ribeiro, P. Neto, C. Pinho, Mean porosity and pressure drop measurements in packed beds of monosized spheres: side wall effects, International Review of, Chem. Eng. 2 (2010) 40–46. https://www.researchgate.net/publication/303213122.

[41] M. Antil, S. Singh, M. Baghat, V. Vilvas, S. Sundaramurthy, Column optimization of adsorption and evaluation of bed parameters-based on removal of arsenite ion using rice husk, Environ. Sci. Pollut. Res. 29 (2022) 72279–72293, https://doi.org/10.1007/s11356-022-20580-9.

[42] M.D. Yahya, H. Abubakar, K.S. Obayomi, Y.A. Iyaka, B. Suleiman, Simultaneous and continuous biosorption of Cr and Cu (II) ions from industrial tannery effluent using almond shell in a fixed bed column, Results Eng. 6 (2020) 100–113, https://doi.org/10.1016/j.rineng.2020.100113.

[43] O. Levenspiel, Ingeniería de las reacciones químicas, first ed., Reverté, Barcelona, 2009.

[44] E. Wilson, J. Geankoplis, Liquid Mass Transfer at Very Low Reynolds Numbers in Packed Beds, Ind. Eng. Chem. Fundamen. 5 (1966) 9–14, https://doi.org/10.1021/i160017a002.

[45] E. Maucci, C. Briens, R. Matinuzzi, G. Wild, Modeling of transient particle–liquid mass transfer in liquid and liquid–solid systems, Chem. Eng. Sci. 56 (2001) 4555–4570, https://doi.org/10.1016/S0009-2509(00)00461-9.

[46] E. Glueckauf, Theory of chromatography part lo.-formula for diffusion into spheres and their application to chromatography, Trans. Faraday Soc. 51 (1955) 1540–1551, https://doi.org/10.1039/TF9555101540.

[47] C.V. Diniza, V.S.T. Ciminellia, F.M. Doyleb, The use of the chelating resin Dowex M-4195 in the adsorption of selected heavy metal ions from manganese solutions, Hydrometallurgy 78 (2005) 147–155, https://doi.org/10.1016/j.hydromet.2004.12.007.

[48] A.L. Riley, S.E. Pepper, E.L. Sexton, M.D. Ogden, Metal Removal from Synthetic Mine Tailing Leachates using Fixed-Bed Ion-Exchange Columns, Conference Paper, July 2018.

[49] J. Carrillo-Abad, M. Garcia-Gabaldon, I. Ortiz-Gandara, E. Bringas, A.M. Urtiaga, I. Ortiz, V. Perez-Herranz, Selective recovery of zinc from spent pickling baths by the combination of membrane-based solvent extraction and electrowinning technologies, Separ. Purif. Technol. 151 (2015) 232–242, https://doi.org/10.1016/j.seppur.2015.07.051.

[50] A.Y.M. Al-Murshedi, J.M. Hartley, A.P. Abbott, K.S. Ryder, Effect of water on the electrodeposition of copper on nickel in deep eutectic solvents, Int. J. Surf. Eng. Coatings 97 (2019) 321–329, https://doi.org/10.1080/00202967.2019.1671062.

[51] B. Yang, S. Jiang, C. Zhang, G. Zhao, M. Wu, N. Xiao, P. Su, Recovery of iron from iron-rich pickling sludge for preparing P-doped polyferric chloride coagulant, Chemosphere 283 (2021) 131–216, https://doi.org/10.1016/j.chemosphere.2021.131216.

[52] B. Mwewa, S. Stopic, S. Ndlovu, G.S. Simate, B. Xakalashe, B. Friedrich, Synthesis of Poly-Alumino-Ferric Sulphate Coagulant from Acid Mine Drainage by Precipitation, Metals 9 (2019) 1166, https://doi.org/10.3390/met9111166.